Experimental Cell Research 452 (2025) 114730

Contents lists available at ScienceDirect

Experimental Cell Research

journal homepage: www.elsevier.com/locate/yexcr

Research article

NudCL2 suppresses pancreatic cancer progression by inhibiting SLC7A11-mediated EMT and metastasis

Jiaxing Feng [a,1], Mingyang Yang [a,1], Rijin Lin [a], Kaifeng Shang [a], Meng Sun [a], Zijie Guo [a], Yanting Wang [a], Tianhua Zhou [a,b,d,*], Feng Yang [c,**], Yuehong Yang [a,b,***]

[a] Institute of Gastroenterology of the Second Affiliated Hospital, Department of Cell Biology, Zhejiang University School of Medicine, Hangzhou, 310009, China
[b] Center for Medical Research and Innovation in Digestive System Tumors, Ministry of Education, Hangzhou, 310058, China
[c] Binjiang Institute of Zhejiang University, Hangzhou, 310053, China
[d] Center for RNA Medicine, International Institutes of Medicine, the Fourth Affiliated Hospital of Zhejiang University School of Medicine, Yiwu, 322000, China

ARTICLE INFO

Keywords:
NudCL2
Pancreatic cancer (PC)
SLC7A11
EMT

ABSTRACT

Pancreatic cancer (PC) is a highly aggressive malignancy with limited therapeutic options and poor prognosis. NudC-like protein 2 (NudCL2), a molecular cochaperone of HSP90, has been implicated in various cellular processes; however, its role in pancreatic cancer remains poorly understood. In this study, we report that NudCL2 expression is significantly downregulated in PC tissues and is correlated with poor patient survival. The results of functional assays revealed that NudCL2 knockdown enhances cell invasion and migration *in vitro* and promotes lung and liver metastases *in vivo*. Further analysis revealed solute carrier family 7 member 11 (SLC7A11) as a key downstream effector that was upregulated upon NudCL2 depletion. Suppression of SLC7A11 reversed the increase in cell motility induced by NudCL2 depletion. Mechanistically, our findings suggest that NudCL2 regulates the transcriptional activity of SLC7A11 and that the NudCL2/SLC7A11 axis may suppress cell motility by inhibiting the epithelial-mesenchymal transition (EMT) pathway. Collectively, these results highlight the important role of NudCL2 in PC progression through the modulation of EMT via SLC7A11, providing valuable insights into its potential as both a therapeutic target and a prognostic biomarker.

1. Introduction

Pancreatic cancer (PC), primarily pancreatic ductal adenocarcinoma (PDAC), is among the most aggressive malignancies and has a dismal prognosis [1–3]. Owing to its deep anatomical location and lack of early clinical symptoms, most patients are diagnosed at advanced stages with distant metastasis [4]. Only 10–15 % of patients are eligible for potentially curative surgery, yet the risk of recurrence remains high even after resection [5]. Although numerous molecular drivers of PC have been identified, effective therapeutic targets are still lacking.

Epithelial-mesenchymal transition (EMT) is a key biological process in which epithelial cells undergo loss of polarity and disruption of cell-cell adhesion and acquire mesenchymal features that enhance cellular motility, invasiveness, and resistance to apoptosis [6,7]. EMT is characterized by the downregulation of epithelial markers such as E-cadherin (also known as CDH1) and zonula occludens-1 (ZO-1) and the upregulation of mesenchymal markers such as N-cadherin (CDH2) and vimentin, accompanied by a morphological shift toward a spindle-shaped fibroblast type with increased motility and invasive potential. This process is regulated by transcription factors such as Snail, Twist, and ZEB and by signaling pathways such as the TGF-β, Wnt, Notch, and NF-κB pathways [8–12]. However, the molecular mechanisms driving EMT in PC remain poorly understood.

NudC-like protein 2 (NudCL2), a member of the nuclear distribution protein C (NudC) family, was initially identified by our team as a molecular cochaperone of heat shock protein 90 (HSP90). Our studies demonstrated that NudCL2 plays important roles in several cell

* Corresponding author. Institute of Gastroenterology of the Second Affiliated Hospital, Department of Cell Biology, Zhejiang University School of Medicine, Hangzhou, 310009, China.
** Corresponding author.
*** Corresponding author. Institute of Gastroenterology of the Second Affiliated Hospital, Department of Cell Biology, Zhejiang University School of Medicine, Hangzhou, 310009, China.
E-mail addresses: tzhou@zju.edu.cn (T. Zhou), 11718062@zju.edu.cn (F. Yang), yhyang@zju.edu.cn (Y. Yang).
[1] These authors contributed equally to this work: Jiaxing Feng and Mingyang Yang.

https://doi.org/10.1016/j.yexcr.2025.114730
Received 22 April 2025; Received in revised form 24 August 2025; Accepted 31 August 2025
Available online 2 September 2025

Abbreviations

PC	pancreatic cancer
NudCL2	NudC-like protein 2
HSP90	heat shock protein 90
EMT	epithelial-mesenchymal transition
SLC7A11	solute carrier family 7 member 11

biological processes, namely, cell cycle regulation, migration, and ciliogenesis [13–18]. NudCL2 regulates centriole duplication and sister chromatid cohesion by stabilizing HERC2 (HECT and RLD domain-containing E3 ubiquitin protein ligase 2) and cohesin subunits and by maintaining cytokinesis via the regulator of chromosome condensation 2 (RCC2) [13–15]. Furthermore, NudCL2 is involved in cell migration regulation through the stabilization of LIS1 (lissencephaly 1) and myosin-9 [16,17]. NudCL2 also functions as an autophagy receptor, mediating the selective degradation of the mother centriole-capping protein CP110 to promote ciliogenesis [18]. Despite its diverse cellular functions, the role of NudCL2 in human disease, particularly in cancer, remains largely uncharacterized.

In this study, we provide evidence that NudCL2 plays a critical role in PC. Our data revealed that the expression of NudCL2 is significantly downregulated in PC tissues and that this downregulation is correlated with advanced disease progression and poor patient outcomes. Furthermore, we demonstrated that NudCL2 functions as a negative regulator of EMT by inhibiting SLC7A11 expression, thereby suppressing cell motility and metastasis. These findings not only elucidate the molecular mechanisms underlying PC but also underscore the potential of NudCL2 as a promising therapeutic target and prognostic biomarker.

2. Materials and methods

2.1. Cell culture

PANC-1 and PaTu8988t cells were obtained from Procell (Wuhan, China), and the STR test was performed by Procell. The cells were cultured with Dulbecco's modified Eagle's medium (DMEM) containing 10 % FBS (Excell) at 37 °C in 5 % CO_2.

2.2. Human specimens

The cohort tissue array was purchased from Shanghai Biochip. The cohort contains 76 paired of tumor and non-tumor issues, and additional 6 tumor issues. The study was approved by the ethics committee of Shanghai Outdo Biotech Company (YB M-05-01).

2.3. Mice

All procedures involving in mice were approved by the Institutional Animal Care and Use Committee of Zhejiang University (ZJU20250025). NSG mice (5–6 weeks) bred in specific pathogen-free facilities were used for the indicated studies and divided into different groups randomly.

2.4. siRNAs and shRNA

All small interfering RNAs (siRNAs) were synthesized by Gene Pharma. The sequences of the sense strands of the siRNA duplexes are as follows:

NudCL2-1: 5-ACCUUGAGAAAUAACUGCUTT-3.
NudCL2-2: 5-CAAGGGCAAACUCUUUGAUTT-3.
SLC7A11-1: 5-CCAGAUAUGCAUCGUCCUUTT-3.
SLC7A11-2: 5-CCAGGUGGUUUAGAAUAAUTT-3.

To stably knockdown NudCL2, siNudCL2-2 oligo was inserted into the pLKO.1vector. The virus was produced in HEK293T cells by Tsingke Biotechnology (Beijing, China).

2.5. Antibodies

For western blotting analysis, we employed primary antibodies against NudCL2 (1:1,000, 21205-1-AP, Proteintech), E-cadherin (1:1,000, 10681-1-AP, Proteintech), ZO-1 (1:1,000, 33–9100, Thermo Fisher), β-actin (1:2,000, 60004-1 Ig, Proteintech), Vimentin (1:1,000, 10960-1-AP, Proteintech), EDIL3 (1:1,000, sc-293337, Santa cruz), SLC7A11 (1:1,000, F0517, Selleck), ALDH3B1 (1:1,000, BD-PT0190, Biodragon).

For immunofluorescence experiments, we used the following primary antibodies: F-actin (1:200, P1951, Sigma), ZO-1 (1:200, 33–9100, Thermo Fisher), Vimentin (1:200, 10960-1-AP, Proteintech).

2.6. Quantitative real-time RT-PCR

Total RNA was extracted using Trizol reagent (Invitrogen, USA) and reversed by PrimeScript RT Reagent Kit (Vazyme) according to the manufacturer's protocol. Quantitative RT-PCR analyses were performed using ROCHE LightCycler®480 System (Rotor gene 6000 Software, Sydney, Australia) with HiScript Q RT SuperMix (Vazyme). All of the reactions were performed at least three times. *U6* was used as an internal control. The primers used to amplify the target genes were as follows:

NudCL2: Forward: 5-ATCTTTACGGCAGGAGCTGG-3;
Reverse: 5-CTGGTAGCTGCAGCGGTATG-3;
SLC7A11: Forward: 5-TCTCCAAAGGAGGTTACCTGC-3,
Reverse: 5-AGACTCCCCTCAGTAAAGTGAC-3;
pre-*SLC7A11*: Forward: 5-ATTCAGACCAAAGGAGGCAGTT-3,
Reverse: 5- ACATGACATGCATGTGTCTAACC-3;
U6: Forward: 5-CTCGCTTCGGCAGCACA-3,
Reverse: 5- AACGCTTCACGAATTTGCGT-3.

2.7. Western blotting

Immunoblotting was performed using standard protocols. Briefly, cells were washed with PBS and lysed in ice-cold TBSN buffer (20 mM Tris [pH 8.0], 150 mM NaCl, 0.5 % Nonidet P-40, 5 mM EGTA, 1.5 mM EDTA, 0.5 mM Na3VO4, 20 mM p-nitrophenyl phosphate) containing a protease inhibitor cocktail (Selleck, B14002). After 10 min of incubation on ice, lysates were centrifuged at 12,000 rpm for 10 min at 4 °C to remove insoluble material. The resulting supernatants were mixed with SDS loading buffer and denatured by boiling at 95 °C for 10 min. Protein samples were separated by SDS-PAGE using 8 %, 10 %, or 12 % polyacrylamide gels as appropriate, then transferred to PVDF membranes (Millipore). Membranes were blocked with 5 % BSA in TBST for 1 h at room temperature followed by incubation with primary antibodies and subsequently with HRP-conjugated secondary antibodies (Cell Signaling Technology). Protein bands were detected using a chemiluminescent immunoassay analyzer (Bio-Rad).

2.8. Immunofluorescence (IF)

For IF in Fig. 7, Patu8988t cells were seeded on coverslips. When the cells reached 80–90 % confluency, they were washed with PBS and then fixed with 4 % paraformaldehyde for 30 min at room temperature. The coverslips were washed three times with PBST solution (1 x PBS and 0.1 % Triton X-100) for 5 min each time followed by incubation with 3 % BSA solution (1x PBS, 0.1 % Triton X-100 and 3 % BSA) for 30 min. Cells were incubated with primary antibodies diluted in 3 % BSA solution (1:200) as indicated in the text, for 2 h at room temperature or overnight at 4 °C. Then, cells were washed by PBST three times for 5 min, followed by incubation with Alexa Fluor 555 and Alexa Fluor 488-conjugated secondary antibodies diluted in 3 % BSA solution (1:200) at room temperature for 1 h. The mounted coverslips were analyzed by confocal

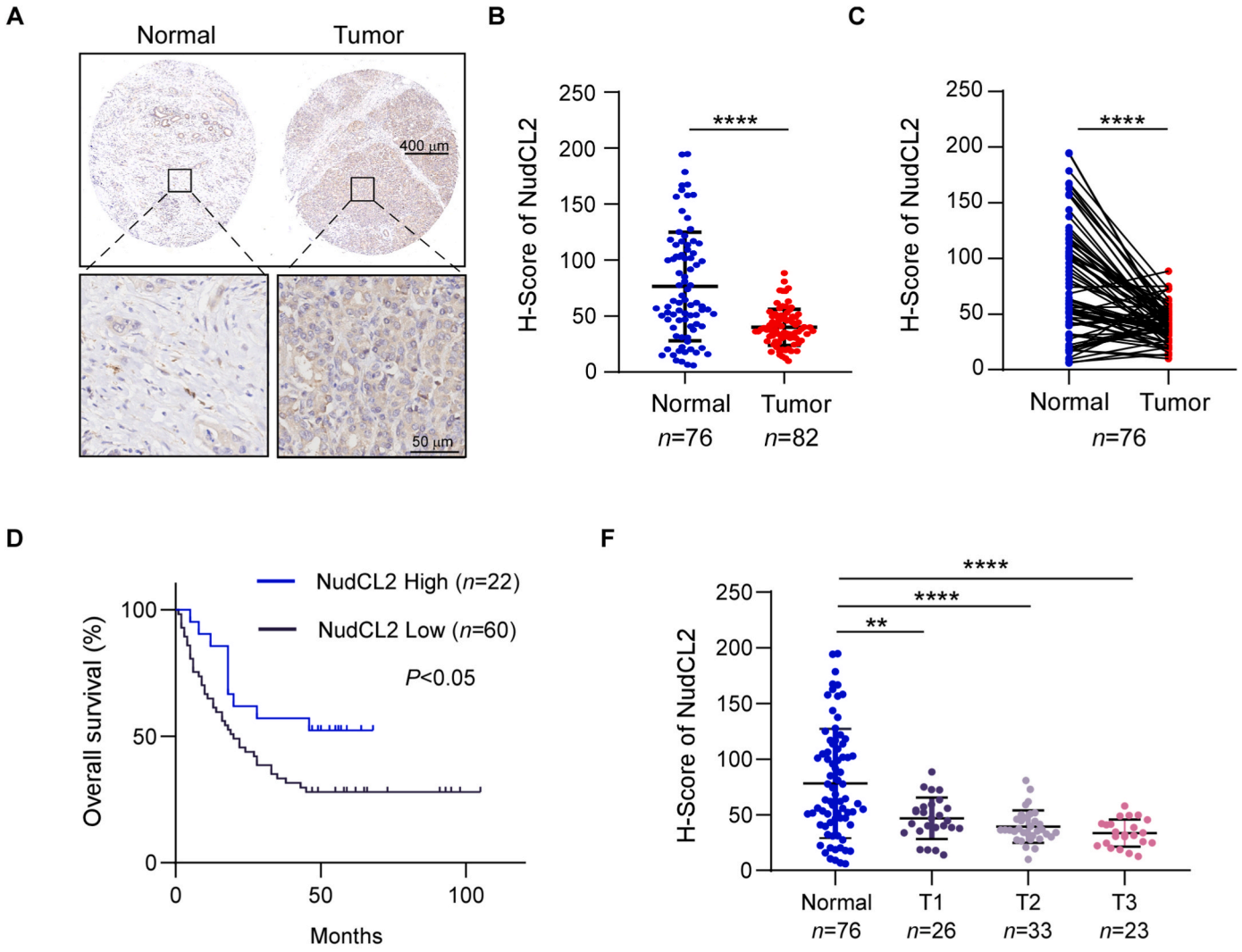

Fig. 1. NudCL2 is downregulated in pancreatic cancer tissues and associated with poor survival (A) Representative immunohistochemical staining images of NudCL2 in PC and paired adjacent normal samples from the tissue microarray are presented. The left panel represents normal paired pancreatic tissue, while the right panel depicts pancreatic cancer tissue. (B) The statistical analysis of H-scores of NudCL2 derived from the immunohistochemical analysis of the tissue array is presented. The cohort contains 76 pairs of matched tissues and an additional 6 tumor tissues. (C) The H-scores of NudCL2 obtained from the immunohistochemical results in the paired tissue array are shown. (D) The Kaplan–Meier method was used to evaluate the correlation between NudCL2 protein expression levels and patient survival in patients with PC. Statistical significance was determined using the log-rank (Mantel–Cox) test. $P < 0.05$. (E) Multivariable risk factor analyses of the cohort. All the bars correspond to 95 % confidence intervals (CIs). HR = hazard ratio. (F) H-scores from the immunohistochemical tissue of normal and PC patients with different tumor stages are shown. The data in B, C, and F are presented as the means ± SDs. Student's *t*-test, $^{**}P < 0.01$, $^{****}P < 0.0001$.

Table 1
Multivariable analyses were performed using Chi-square statistical analysis based on NudCL2 expression and clinical characteristics, including gender, age, pathological grade, T stage, N stage, and M stage.

NudCL2	Feature	Low	High	Chi-square	*P*-value
Gender	male	31	12	0.053	0.817
	female	29	10		
Age	≤65	27	14	2.236	0.135
	>65	33	8		
Pathological grade	G1	12	8	2.506	0.286
	G2	37	10		
	G3	11	4		
T	T1	14	12	7.703	0.021
	T2	26	7		
	T3	20	3		
	T4	0	0		
N	N0	33	14	0.491	0.484
	N1	27	8		
	N2	0	0		
	N3	0	0		
M	M0	56	21	0.127	0.722
	M1	4	1		

fluorescence microscopy with an oil immersion x63 objective (Zeiss, LSM800, USA).

2.9. Animal model

For intravenously metastasis assays, 1×10^5 PaTu8988t cells stably expressing shCtrl or shNudCL2 were resuspended with 100 μL PBS and injected into NSG mice through tail vein, 10 mice were randomly divided into two groups ($n = 5$). Obvious weight loss in mice was used as the endpoint for experiments. For orthotopic pancreatic cancer implantation model of pancreatic cancer, 3×10^6 PaTu8988t cells stably expressing shCtrl or shNudCL2 were mixed with matrix gel and injected into the pancreas through surgery. Each group contains 4 random NSG mice (5–6 weeks). The mice were bred in SPF environment for 21 days and euthanized. For intrasplenic injection model, 5×10^5 PaTu8988t cells stably expressing shCtrl or shNudCL2 were resuspended with 50 μL PBS injected into spleen of NSG mice (5–6 weeks) by surgery ($n = 4$). These studies were approved by the ethics committee of Zhejiang University.

2.10. Cell scratch assay

Patu8988t cells treated with Ctrl or *NudCL2* siRNAs were cultured in 6-well plates and allowed to grow to 80 %–90 % density. Then a white pipette tip was used to make a vertical scratch in the culture well, and the cells were washed with PBS solution three times to remove free cells. The cells were then starved of serum in fresh medium to minimize the influence of cell proliferation on the results of the experiment. Images of the scratched area were taken at different time points such as 0 h and 24 h (a small circle is marked on the bottom of the plate with a marker pen to ensure that the same point is captured in each image). The experiment was repeated at least 3 biological replicates, and 1 time of representative result is shown in the figures.

2.11. Migration and invasion assays

For the migration assay, cells were harvested, centrifuged, and resuspended in serum-free medium. A total of 30,000 cells were taken, and diluted with 200 μL serum-free medium. Then the diluted cells and added to the upper chamber of the transwell plate. In the lower chamber of the transwell, 800 μL of medium supplemented with 10 % serum was added to ensure contact between the medium and the bottom of the upper chamber. For invasion assay, 50 μL of 5 % gelatin was added into the upper chamber The assembly was placed in a 5 % CO_2 incubator at 37 °C for 36 h or 48 h, the upper chamber of transwell plate for 2 h before adding the diluted cells. About incubation for 24 h, the upper chamber was removed, stained with crystal violet, and the cells on the upper chamber that had not migrated were carefully wiped off with a cotton swab. The cells that had migrated to the back side were observed and recorded, and photographs were taken. Each experiment was repeated at least 3 biological replicates, and 1 time of representative result is shown in the figures.

2.12. RNA sequencing

Ctrl or NudCL2-deficient Patu8988t cells were harvested and total RNA was extracted. An mRNA sequencing library was subsequently prepared using the T7 amplification platform (Novogene). Sequencing and bioinformatics analyses were performed by Majorbio (Shanghai, China). HISAT2 was employed to align the filtered reads to the human reference genome. The mapping results, stored in BAM format, were quantified using the feature Counts function from the Rsubread package in R. Although the counting process utilized human genome annotations for comparison, downstream analyses were exclusively performed on human data. Differential gene expression analysis was carried out using DESeq2, with a threshold of Log2 (fold change) > 1 applied to identify significantly altered genes. The resulting gene list was further curated through an integrative approach, combining with literature review and functional annotation (known or predicted) via UniProt. The mRNA sequencing data generated in this study are publicly available when published in the Sequence Read Archive (SRA) database at PRJNA1300627.

2.13. Luciferase reporter assay

For SLC7A11-promoter activity assay, the upstream −2000~50 bp of the promoter of SLC7A11 was conducted into PGL3 vector. Patu8988t cells treated with Ctrl or *NudCL2* siRNAs were co-transfected with pGL3 basic/pGL3-SLC7A11 promoter and TK-renilla vector for 24 h. Luciferase assays were measured using Dual-Luciferase Reporter System (Promega, Fitchburg, WI, USA) according to the manufacturer's protocol. The transfection efficiency data were normalized by comparing Firefly luciferase activity to that of Renilla luciferase. All assays were independently conducted in triplicate.

2.14. mRNA and protein stability assay

Patu8988t cells transfected with the indicated siRNAs were treated with actinomycin D (MCE, China, 10 μg/mL) to block subsequent RNA synthesis, or Cycloheximide (CHX, MCE, China, 100 μg/mL) to inhibit protein synthesis. Cells were collected at specified time points, and total RNA or protein was extracted. The residual mRNA levels of *SLC7A11* in each group were quantified using quantitative RT-PCR, and the protein level were detected by western blot. The RNA or protein levels at each time point were normalized relative to the level measured at the initial time point (0 h). Each assay was performed independently in triplicate.

2.15. Statistics

Data are representative of at least three independent experiments. GraphPad Prism 8.3 software was used to perform statistical analysis. Means and standard deviations (SD) were calculated and shown in the graphs. Student's *t*-test was used to determine statistically significant differences between two groups. The Kaplan-Meier method was applied to analyze the correlation between the expression levels of NudCL2 protein and the survival status of patients with pancreatic cancer. Forest plots depicting the results of the multivariate analysis of prognostic factors associated with overall survival were constructed based on a multivariate Cox proportional hazards regression model. Patients were stratified into high-expression and low-expression groups according to an optimal cutoff value, which was determined using a previously

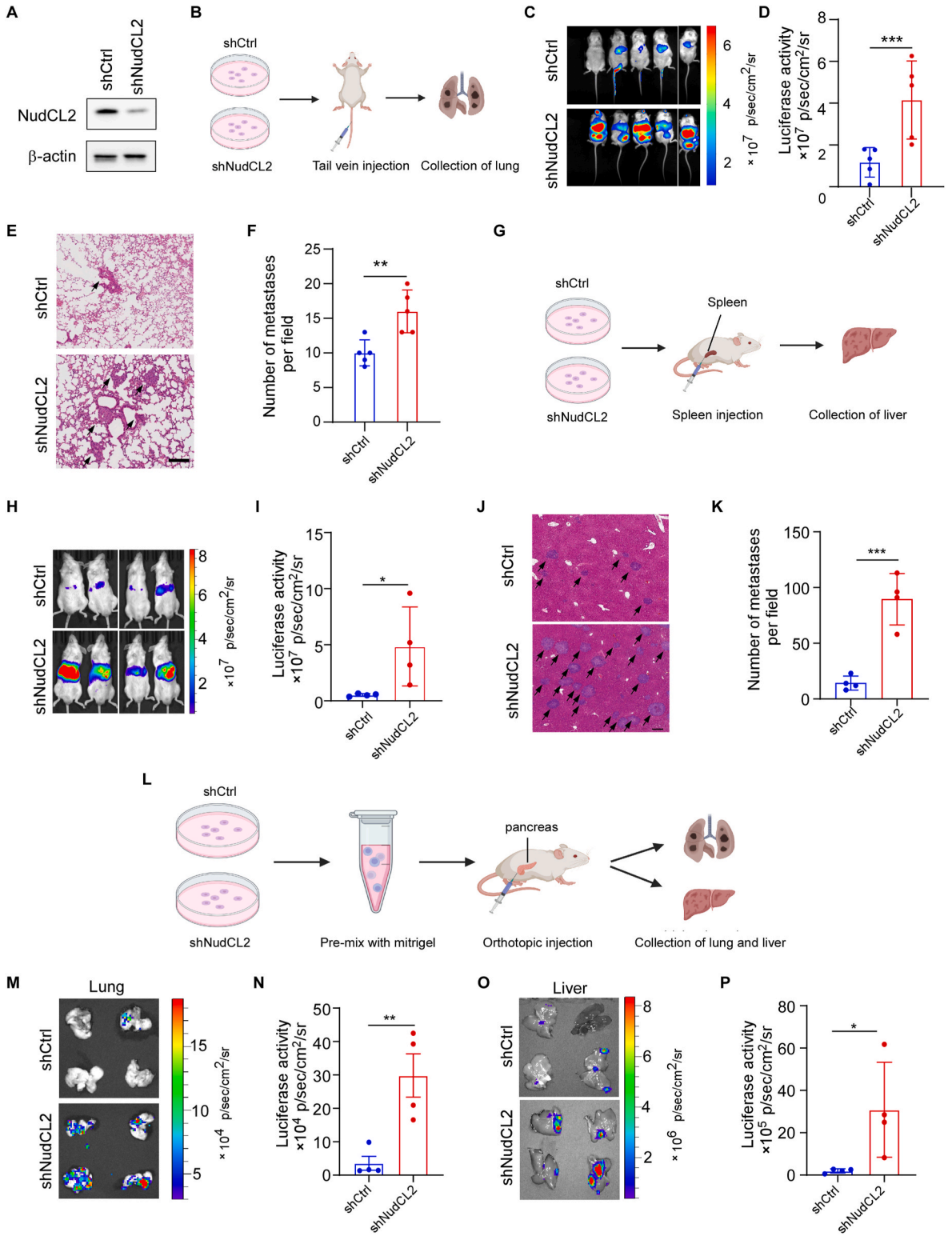

Fig. 2. NudCL2 knockdown promotes metastases of PC cells *in vivo* (A) Western blots of NudCL2 expression in shCtrl and shNudCL2 Patu8988t cells. (B) shCtrl and shNudCL2 PaTu8988t cells were intravenously injected into NSG mice ($n = 5$). (C) Representative bioluminescence images are presented. (D) Quantification analyses of bioluminescent images of metastases are shown. (E) Representative H&E images of lung metastases (black narrows). Scale bar, 250 μm. (F) Statistical analyses of the number of metastatic nodules in the lung are shown. (G) shCtrl or shNudCL2 Patu8988t cells were injected into the spleen of NSG mice ($n = 4$) for 21 days. (H) Representative bioluminescent images of metastasis in the shCtrl and shNudCl2 groups. (I) Quantification analyses of bioluminescent images of liver metastases are shown. (J) Representative H&E images of liver metastases (black narrows) are shown. Scale bars, 250 μm. (K) Statistical analyses of the number of metastatic nodules are shown. (L) shCtrl or shNudCL2 Patu8988t cells were injected *in situ* into the pancreas of NSG mice ($n = 4$) for 21 days. (M, O) Bioluminescent images of mouse lungs (M) and livers (O). (N, P) Statistical analyses of bioluminescent images of mouse lungs (N) and livers (P). All the data are shown as the means ± SDs. Student's *t*-test, $^*P < 0.05$, $^{**}P < 0.01$, $^{***}P < 0.001$. B, G, and L were created with BioRender.com.

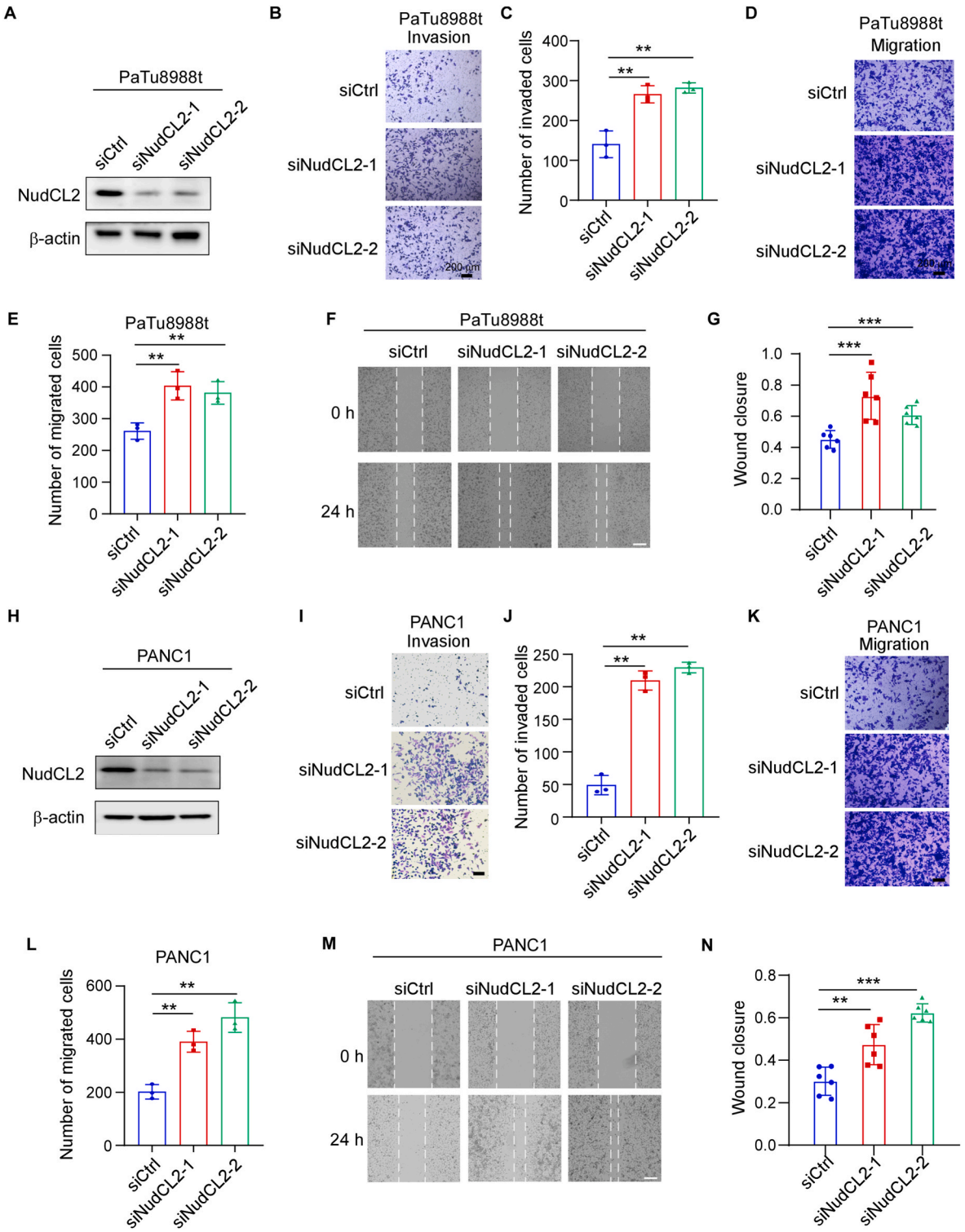

Fig. 3. Knockdown of NudCL2 enhances the aggressiveness of pancreatic cancer cells (A–G) PaTu8988t cells were transfected with Ctrl and *NudCL2* siRNAs and subjected to invasion and migration assays and wound healing assays. The levels of NudCL2 protein were detected by western blot (A). Representative images of the invasion (B) and migration (D) assays and data analyses (C, E) are shown. Scale bar, 200 μm. Representative images (F) of the wound healing assay and data analyses (G) are shown. (H–N) PANC1 cells treated with Ctrl and *NudCL2* siRNAs were subjected to invasion and migration assays. NudCL2 protein levels were detected by western blot (H). Representative images of the invasion (I) and migration (K) assays and data analyses (J, L) are shown. Representative images (M) of the wound healing assay and data analyses (N) are shown. The data are shown as the means ± SDs. Student's *t*-test, $^{**}P < 0.01$, $^{***}P < 0.001$.

established algorithm. The Chi-square statistical test was used to determine the associations between NudCL2 expression and clinicopathological parameters. Two-way Anova was employed to analysis RNA and protein stability of SLC7A11. $^{*}P < 0.05$ indicates statistical significance.

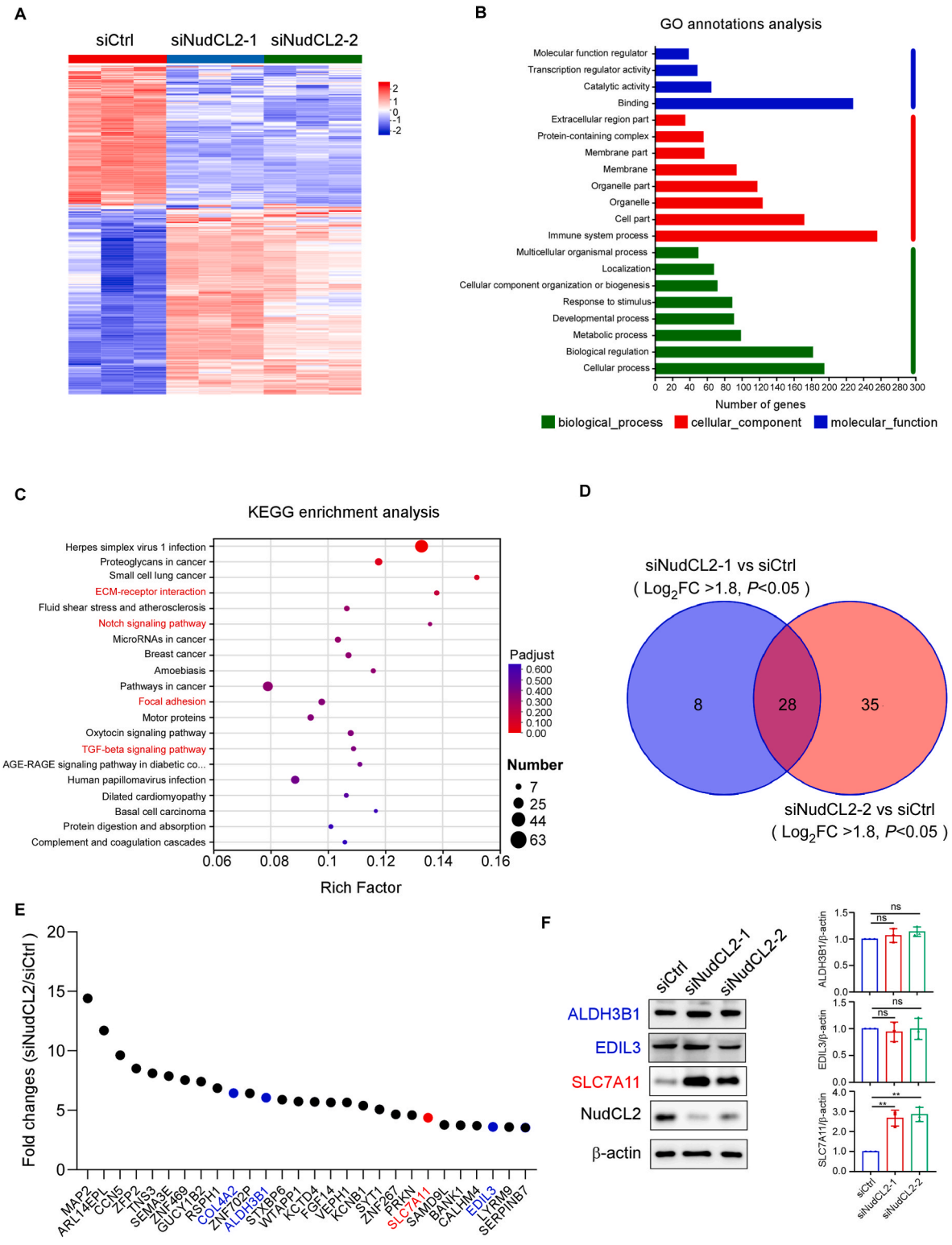

Fig. 4. Identification of SLC7A11 as a downstream target of NudCL2 (A) Patu8988t cancer cells were transfected with Ctrl or *NudCL2* siRNAs for 48 h, followed by mRNA sequencing. A heatmap was generated to display genes that were differentially expressed between NudCL2-depleted cells and control cells. (B) The GO-cellular components of the siCtrl, siNudCL2-1, and siNudCL2-1 groups are presented. (C) KEGG enrichment analysis of siCtrl, siNudCL2-1, and siNudCL2-1. (D) Venn diagram showing the overlapping mRNAs in Patu8988t cells treated with *NudCL2* siRNAs (Log_2 FC > 1.8). (E) List of mRNAs whose expression changed in NudCL2-depleted Patu8988t cells. The data are presented as the fold change in peak intensity (siNudCL2-1/siCtrl) (F) Western blots of the indicated proteins in Patu8988t cells treated with *NudCL2* siRNAs. The gray values were measured with ImageJ. The data are presented as the means ± SDs. Student's *t*-test, $^{**}P < 0.01$; ns, no significance.

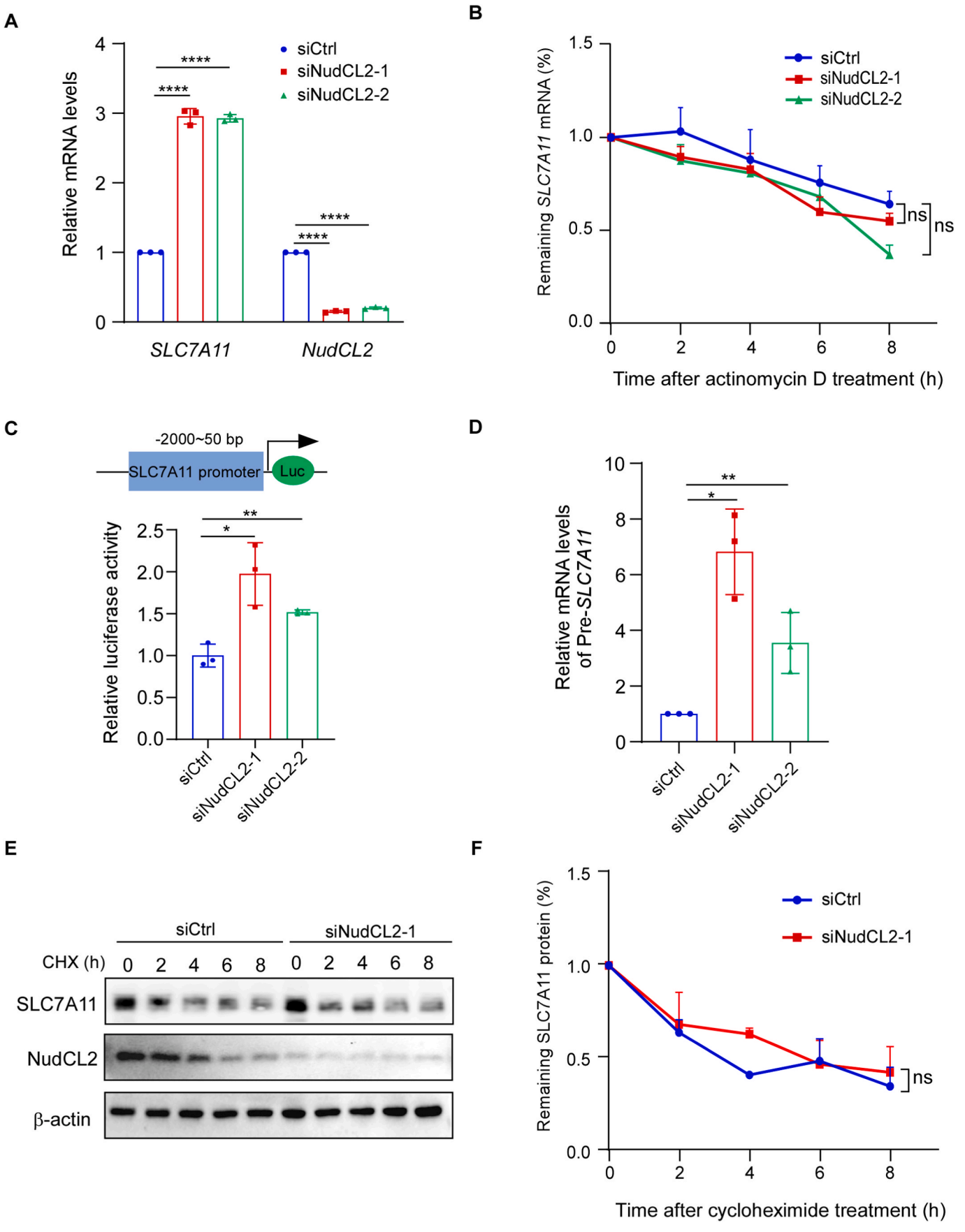

(caption on next page)

Fig. 5. NudCL2 knockdown increases the transcriptional activity of SLC7A11 (A) Patu8988t cells treated with *NudCL2* siRNAs or Ctrl siRNA were subjected to RT–PCR. (B) Patu8988t cells were treated with *NudCL2* siRNAs for 48 h. The remaining *SLC7A11* mRNAs were analyzed by quantitative RT–PCR at the indicated time points after actinomycin D treatment. Two-way ANOVA. (C) Dual-luciferase reporter assay showing the effects of NudCL2 depletion on relative SLC7A11 promoter (−2000bp ~50bp) activity in the Patu8988t cells. (D) Quantitative RT–PCR analysis of precursor *SLC7A11* mRNA expression in Patu8988t cells with Ctrl or NudCL2 depletion. Data from three independent experiments (A, C, D) are shown as the means ± SDs. Student's *t*-test, $*P < 0.05$, $**P < 0.01$, $****P < 0.0001$. (E) Patu8988t cells transfected with *NudCL2* siRNAs were treated with cycloheximide for the indicated times and subjected to western blot analysis. (F) Quantitative data from three independent experiments of (E) are shown as the means ± SDs. Two-way ANOVA; ns, no significance.

3. Results

3.1. NudCL2 is downregulated in pancreatic cancer and associated with poor prognosis

To assess the clinical relevance of NudCL2 in pancreatic cancer, we performed immunohistochemical staining on tissue microarrays containing pancreatic cancer tissues and matched adjacent noncancerous tissues. H-score analysis revealed a significant reduction in NudCL2 protein levels in tumor tissues, with 69.73 % (53/76) of cases showing downregulation compared with adjacent normal tissues (Fig. 1A–C). H-score analysis revealed a significant reduction in NudCL2 protein levels in tumor tissues, with 69.73 % (53/76) of cases showing downregulation compared with matched adjacent normal tissues (Fig. 1C). Furthermore, survival analysis indicated that low NudCL2 expression was significantly associated with lower overall survival (Fig. 1D). Multivariate Cox regression analysis demonstrated that low NudCL2 expression served as an independent negative prognostic factor for predicting the clinical outcomes of pancreatic cancer patients (Fig. 1E).

We further classified 82 pancreatic cancer samples into high ($n = 22$) and low ($n = 60$) NudCL2 expression groups and evaluated their correlations with clinicopathological features. Low NudCL2 expression was significantly associated with greater invasion depth (T stage) (Table 1). Notably, a significant reduction in NudCL2 protein levels occurred as early as the T1 stage, with consistently low levels maintained through the T2 and T3 stages (Fig. 1F). These data suggest that NudCL2 downregulation is associated with tumor progression and poor prognosis in pancreatic cancer.

3.2. Depletion of NudCL2 enhances the metastasis potential and migratory capacity of PC cells

To investigate the role of NudCL2 in pancreatic cancer metastasis, we conducted a series of *in vivo* and *in vitro* experiments. In a tail vein metastasis model, compared with control mice (shCtrl), mice injected with NudCL2-depleted PaTu8988t cells (shNudCL2) exhibited significantly greater metastatic burdens in the lungs and liver, as confirmed by gross morphology and histological analysis (Fig. 2A–F). Additionally, to assess liver-tropic metastatic behavior via hematogenous dissemination, we employed an intrasplenic injection model. Again, mice injected with NudCL2-deficient cells exhibited a significantly higher metastatic burden in the liver, as measured by imaging, histology, and nodule quantification (Fig. 2G–K). These data indicate NudCL2 plays an important role in pancreatic cancer metastases. To more accurately recapitulate spontaneous pancreatic cancer metastases, we conducted an orthotopic pancreatic cancer implantation model, wherein Patu8988t cells stably expressing either control shRNA or shRNA targeting *NudCL2* were injected directly into the pancreas of immunodeficient NSG mice. After 21 days, bioluminescence imaging analysis revealed that NudCL2-depleted tumors exhibited markedly enhanced metastases to both the lung and liver compared to controls, supporting a key role for NudCL2 in suppressing systemic spread from the primary site (Fig. 2L–P).

To further explore the underlying cellular mechanisms, we assessed the impact of NudCL2 knockdown on cell behavior. Transwell invasion assays revealed that depletion of NudCL2 markedly increased the invasive capacity of both PANC-1 and PaTu8988t cells (Fig. 3A–C, H–J). Similarly, wound healing and migration assays revealed enhanced migratory ability in NudCL2-deficient cells (Fig. 3D–G, K–N). These results collectively demonstrate that NudCL2 functions as a negative regulator of pancreatic cancer metastasis by suppressing cell invasion and migration.

3.3. SLC7A11 is a downstream target of NudCL2 in PC cells

To further elucidate the functional role of NudCL2 in PC, we performed RNA sequencing analysis on PaTu8988t cells transfected with siCtrl, siNudCL2-1, or siNudCL2-2. A total of 340 differentially expressed genes ($|\text{fold change}| > 2$, $P < 0.05$) were consistently altered in both NudCL2 knockdown groups compared with the control group, as shown in the heatmap (Fig. 4A). Gene Ontology (GO) enrichment analysis and KEGG pathway analyses revealed that NudCL2 depletion affected multiple pathways associated with cell motility (Fig. 4B and C), such as Notch signaling, ECM-receptor interaction, focal adhesion, and TGF-β signaling [11,19–22]. These findings suggest that NudCL2 plays a regulatory role in genes involved in cellular motility.

To identify the key downstream targets of NudCL2, we conducted a systematic screen for overlapping upregulated mRNAs (Log_2 fold change >1.8) in the two independent knockdown groups and identified 28 genes whose expression was consistently upregulated (Fig. 4D). Among these candidates, ALDH3B1, SLC7A11, and EDIL3 have been previously reported to be associated with pancreatic cancer progression [23–27]. Further western blot analysis revealed that only SLC7A11 protein expression was significantly elevated following NudCL2 knockdown (Fig. 4E and F), suggesting that SLC7A11 may be a prominent downstream target of NudCL2 in PC cells.

3.4. NudCL2 knockdown increases the transcriptional activity of SLC7A11

To investigate the regulatory mechanism of NudCL2 on SLC7A11 expression, we conducted a series of additional experiments to determine whether NudCL2 regulates SLC7A11 expression at the transcriptional, posttranscriptional, or protein level. Using RT–PCR, we first confirmed that *SLC7A11* mRNA levels were significantly increased following NudCL2 knockdown. These findings were consistent with our RNA-seq data (Fig. 5A). To determine whether NudCL2 affects the stability of *SLC7A11* mRNA, we treated Patu8988t cells with actinomycin D to inhibit transcription and measured the remaining mRNA over time. The results revealed that NudCL2 depletion had no effect on *SLC7A11* mRNA degradation kinetics, suggesting that NudCL2 does not regulate the RNA stability of *SLC7A11* (Fig. 5B). We then assessed the promoter activity of *SLC7A11* using a dual-luciferase assay involving the −2000 to +50 bp upstream regulatory region. NudCL2 knockdown significantly increased *SLC7A11* promoter activity (Fig. 5C), indicating transcriptional regulation. RT-PCR targeting precursor *SLC7A11* transcripts further confirmed the increase in transcription upon NudCL2 knockdown (Fig. 5D). Finally, we examined whether NudCL2 affects SLC7A11 protein stability using cycloheximide (CHX) chase assays. Western blotting revealed no difference in SLC7A11 degradation rates over time upon NudCL2 knockdown (Fig. 5E and F). Collectively, these results demonstrate that NudCL2 primarily affects SLC7A11 expression at the transcriptional level rather than through RNA or protein stability.

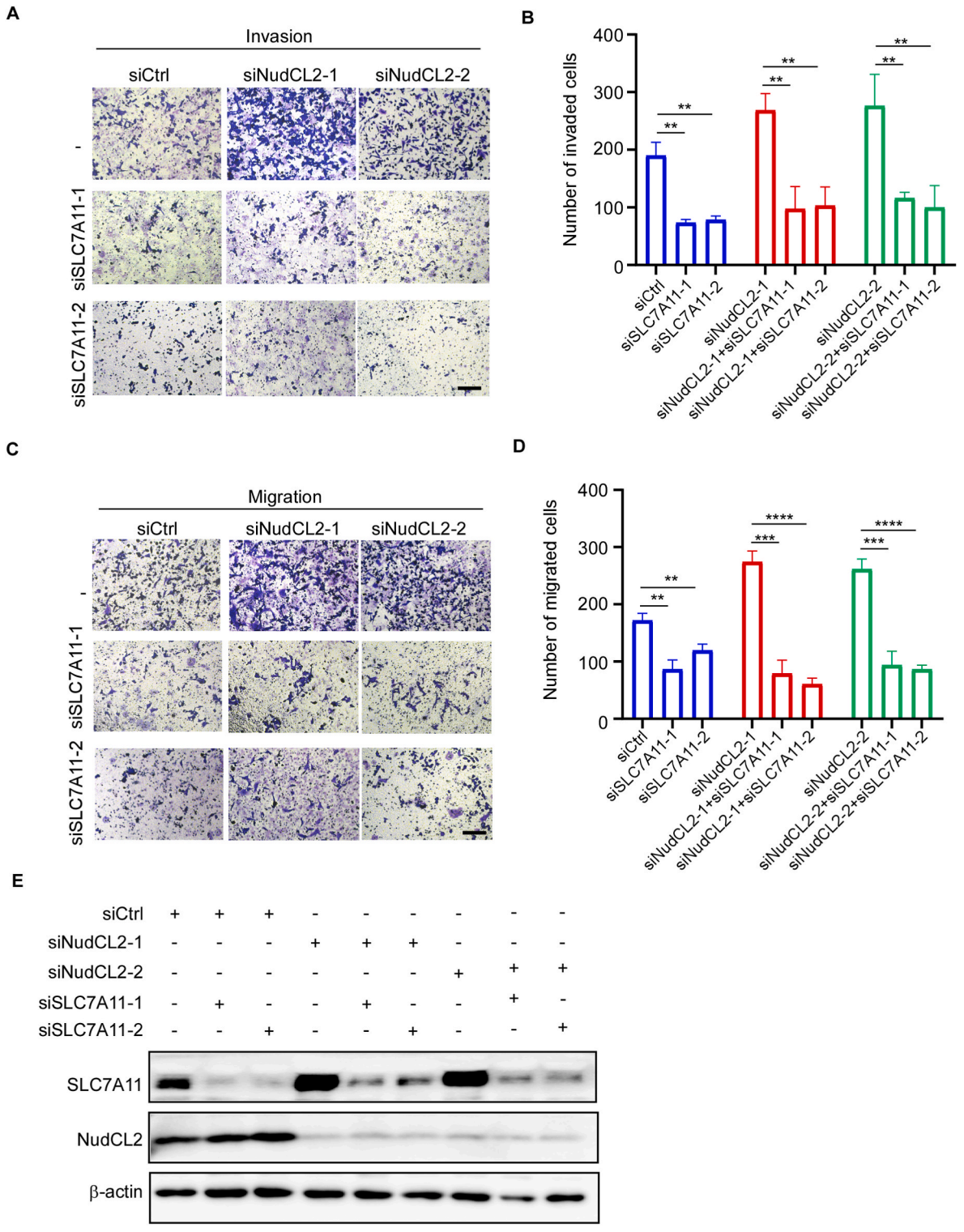

Fig. 6. Downregulation of SLC7A11 expression in NudCL2-depleted cancer cells attenuates increased cell motility (A, B) Patu8988t cells treated with *NudCL2* siRNAs were subjected to invasion assays. Representative images (A) and statistical data (B) are shown. (C, D) Patu8988t cells transfected with *NudCL2* siRNAs were subjected to a migration assay. Representative images (A) and statistical data (B) are presented. Scale bar, 200 μm. (E) Western blots of Patu8988t cells treated with the indicated siRNAs. Data are presented as the means ± SDs; Student's *t*-test, $^{**}P < 0.01$, $^{***}P < 0.001$, $^{****}P < 0.0001$.

3.5. NudCL2 regulates pancreatic cancer cell migration and invasion via SLC7A11

SLC7A11 is known to be upregulated in pancreatic cancer and is associated with poor patient survival [24]. To determine whether SLC7A11 affects NudCL2-driven phenotypes, we assessed its role in NudCL2-depleted pancreatic cancer cells. The downregulation of SLC7A11 expression significantly reduced cell invasion and migration, effectively reversing the enhanced migratory and invasive abilities induced by NudCL2 knockdown (Fig. 6). These findings suggest that SLC7A11 may be a critical downstream effector of NudCL2 in regulating the motility of PC cells.

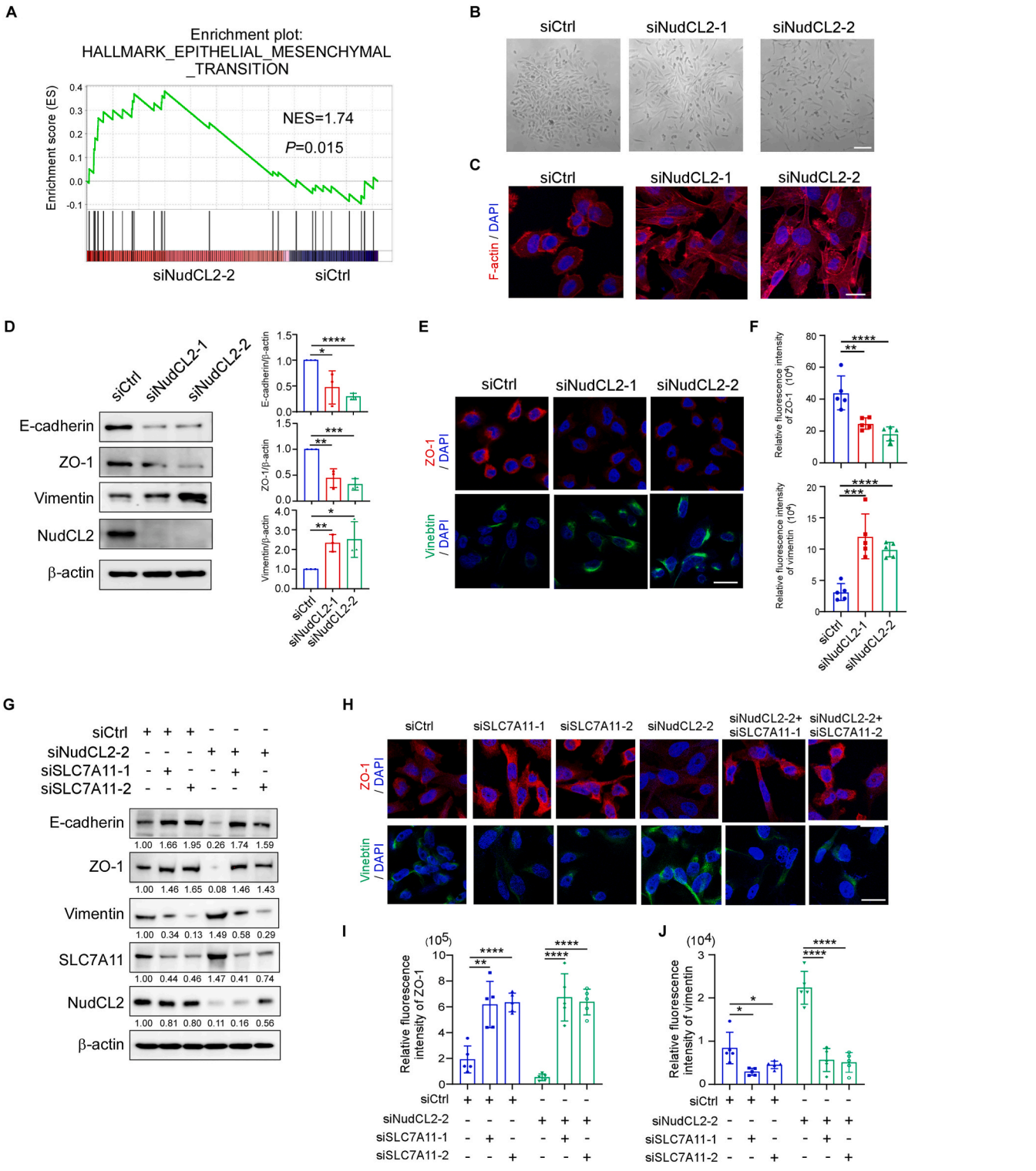

Fig. 7. Depletion of NudCL2 promotes EMT in pancreatic cancer cells by upregulating SLC7A11 expression (A) GSEA results revealing significant enrichment of the epithelial mesenchymal transition in siNudCL2-2 and siCtrl Patu8988t cells. (B) Representative images showing the cell shape of a colony formed by Patu8988t cells treated with *NudCL2* siRNAs. (C) Representative confocal microscopy images of Patu8988t cells treated with *NudCL2* siRNAs. F-actin was stained with Fluor-555 (red), and nuclei were stained with Hoechst (blue). Scale bar = 20 μm. (D) Western blot analysis of total cellular protein levels in Patu8988t cells, with β-actin used as a loading control. Statistical analyses of gray values from three independent experiments are shown. (E) Representative confocal microscopy images of Patu8988t cells treated with *NudCL2* siRNAs. ZO-1 was stained with Fluor-555 (red), vimentin was stained with Fluor-488 (green), and nuclei were stained with Hoechst (blue). Scale bar = 20 μm. (F) The statistical data on the fluorescent intensities in (E) are shown as the means ± SDs. (G) Western blot analysis of protein levels in Patu8988t cells treated with the indicated siRNAs. (H) Representative confocal microscopy images of Patu8988t cells transfected with *NudCL2* siRNAs or *SLC7A11* siRNAs. ZO-1 was stained with Fluor-555 (red), vimentin was stained with Fluor-488 (green), and nuclei were stained with Hoechst (blue). Scale bar = 20 μm. (I, J) Statistical data on the fluorescent intensities in (E). The data are shown as the means ± SDs. Student's *t*-test, $^{**}P < 0.01$, $^{***}P < 0.001$, $^{****}P < 0.0001$.

3.6. NudCL2 plays a vital role in the EMT process in pancreatic cancer cells by upregulating SLC7A11 expression

Previous studies have shown that SLC7A11 contributes to EMT and metastasis in multiple cancer types, including hepatocellular carcinoma, lung cancer, glioblastoma, and pituitary neuroendocrine tumors [25,26,28,29]. Our KEGG pathway analysis further revealed the involvement of EMT-related pathways, such as TGF-β and Notch signaling, in NudCL2-deficient cells (Fig. 4C). Additionally, gene set enrichment analysis (GSEA) confirmed that NudCL2 knockdown enhances the EMT process (Fig. 7A). Morphologically, NudCL2-depleted cells exhibited hallmark features of EMT [30,31], including a transition from a cobblestone-like epithelial morphology to an elongated, spindle-shaped mesenchymal phenotype, accompanied by loss of cell-cell junctions and cell polarity (Fig. 7B and C).

Western blotting and immunofluorescence revealed that NudCL2 knockdown resulted in decreased expression of epithelial markers (E-cadherin and ZO-1) and a concomitant increase in the expression of the mesenchymal marker vimentin (Fig. 7D–F), indicating the activation of EMT. To determine whether this effect is mediated by SLC7A11, we performed rescue experiments. The downregulation of SLC7A11 expression effectively reversed the EMT phenotype, restored epithelial marker expression and mitigated the mesenchymal traits induced by NudCL2 depletion (Fig. 7G–J). Collectively, these results suggest that NudCL2 inhibits EMT in pancreatic cancer cells at least in part by downregulating SLC7A11 expression.

4. Discussion

In this study, we identified NudCL2 as a previously unrecognized suppressor of PC metastasis. Our findings demonstrate that NudCL2 is significantly downregulated in PC tissues and is associated with poor patient survival. Functional assays revealed that NudCL2 depletion enhances the invasive and migratory capacity of pancreatic cancer cells *in vitro* and promotes lung and liver metastases *in vivo*, supporting its role as a negative regulator of tumor progression.

Mechanistically, we identified SLC7A11 as a key downstream effector of NudCL2. Transcriptomic analysis revealed that NudCL2 knockdown significantly upregulated SLC7A11, a cystine/glutamate antiporter previously implicated in tumor progression and redox homeostasis [32]. Consistent with its oncogenic potential, SLC7A11 silencing reversed the increased migratory and invasive phenotypes induced by NudCL2 loss. Notably, rescue experiments further confirmed that SLC7A11 mediates the EMT process driven by NudCL2 depletion, as indicated by changes in cellular morphology and the expression of canonical EMT markers. Our further studies indicated that NudCL2 suppresses SLC7A11 expression mainly at the transcriptional level (Fig. 5). The regulatory mechanism by which NudCL2 influences the transcriptional regulation of SLC7A11 remains to be further elucidated in future studies.

RNA sequencing analysis revealed 28 target genes in NudCL2 knockdown cells. Among these candidates, the protein-coding genes ALDH3B1, SLC7A11, and EDIL3, as well as the long noncoding RNA WTAPP1, have been previously associated with the progression of pancreatic cancer [23–27,33]. According to our findings, SLC7A11 was identified as a key downstream effector of NudCL2. Nevertheless, the involvement of other factors in NudCL2-mediated metastasis could not be entirely ruled out. Among these factors, several regulators have been reported to play important roles in other cancers, such as CCN5 (breast cancer) [34], TNS3 (kidney tumors) [35], SEMA3E (gastric cancer) [36] STXBP6 (non-small cell lung cancer) [37], KCTD4 (esophageal cancer) [38], FGF14 (colorectal cancer) [39], VEPH1 (ovarian cancer) [40], KCNB1 (esophageal squamous cell carcinoma) [41], SYT1 (bladder cancer) [42], ZNF267 (hepatocellular carcinoma) [43], PRKN (breast cancer) [44], SAMD9L (gastric cancer) [45], SERPINB7 (non-small cell lung cancer) [46], and MAP2 (lung squamous cell carcinoma) [47]. However, the biological functions of ARL14EPL, ZFP2, ZNF469, GUCY1B2, RSPH1, ZNF702P, BANK1, CALHM4, and LYRM9 in human cancers have not been extensively studied. Although these factors were not found to be involved in the progression of PC, whether these factors are regulated by NudCL2 and participate in NudCL2-mediated metastases in PC still needs to be explored in the future.

These findings also support a novel link between NudCL2 and EMT, a well-established mechanism contributing to pancreatic cancer metastasis. We observed that NudCL2 knockdown induces EMT-like morphological changes, downregulates the expression of epithelial markers (E-cadherin and ZO-1), and upregulates the expression of the mesenchymal marker vimentin. Importantly, silencing SLC7A11 in NudCL2-deficient cells partially restored epithelial characteristics, suggesting that NudCL2 suppresses EMT through the negative regulation of SLC7A11.

Although NudCL2 has been previously implicated in diverse cellular processes, such as chromosome segregation, cytokinesis, and ciliogenesis [13–18], its role in cancer has remained poorly understood. Our findings extend the functional repertoire of NudCL2 and provide the first evidence of its involvement in pancreatic cancer progression. Furthermore, the identification of the NudCL2-SLC7A11 axis highlights a potential mechanism through which NudCL2 inhibits EMT and metastasis.

CRediT authorship contribution statement

Jiaxing Feng: Writing – review & editing, Validation, Investigation, Conceptualization. **Mingyang Yang:** Investigation, Formal analysis, Data curation. **Rijin Lin:** Visualization, Investigation. **Kaifeng Shang:** Methodology, Investigation. **Meng Sun:** Validation, Software, Investigation. **Zijie Guo:** Visualization, Investigation. **Yanting Wang:** Visualization. **Tianhua Zhou:** Supervision, Funding acquisition. **Feng Yang:** Software, Methodology, Investigation. **Yuehong Yang:** Writing – review & editing, Supervision, Funding acquisition, Formal analysis, Data curation, Conceptualization.

Funding

This study was supported by the National Natural Science Foundation of China (Nos. 32070709, 32270771, and U21A20197), the National Key Research and Development Program of China (2019YFA0802202), and the Higher Education Discipline Innovation Project (also known as the111 Project) (B13026).

Declaration of competing interest

The authors declare no competing interests.

Acknowledgements

We are grateful to Yingying Huang, Jiajia Wang (Core Facilities of Zhejiang University School of Medicine) for their technical support, Qin Han (Center of Cryo-Electron Microscopy of Zhejiang University) for their assistance with confocal laser scanning microscope. We thank Bethany Ruth Villa (Princeton University) for her kind editing work of the manuscript. We would like to express our sincere gratitude to Rong Li, in our laboratory, for her invaluable support and assistance in the area of experimental techniques.

Data availability

Data will be made available on request.

References

[1] A. Vincent, J. Herman, R. Schulick, R.H. Hruban, M. Goggins, Pancreatic cancer, Lancet 378 (2011) 607–620.

[2] E.M. Stoffel, R.E. Brand, M. Goggins, Pancreatic cancer: changing epidemiology and new approaches to risk assessment, early detection, and prevention, Gastroenterology 164 (2023) 752–765.
[3] C. Qin, G. Yang, J. Yang, B. Ren, H. Wang, G. Chen, F. Zhao, L. You, W. Wang, Y. Zhao, Metabolism of pancreatic cancer: paving the way to better anticancer strategies, Mol. Cancer 19 (2020) 50.
[4] T.F. Stoop, A.A. Javed, A. Oba, B.G. Koerkamp, T. Seufferlein, J.W. Wilmink, M. G. Besselink, Pancreatic cancer, Lancet 405 (2025) 1182–1202.
[5] S.A. El-Zahaby, Y.S.R. Elnaggar, O.Y. Abdallah, Reviewing two decades of nanomedicine implementations in targeted treatment and diagnosis of pancreatic cancer: an emphasis on state of art, J Control Release 293 (2019) 21–35.
[6] F.M. Davis, T.A. Stewart, E.W. Thompson, G.R. Monteith, Targeting EMT in cancer: opportunities for pharmacological intervention, Trends Pharmacol. Sci. 35 (2014) 479–488.
[7] M.C. Karlsson, S.F. Gonzalez, J. Welin, J. Fuxe, Epithelial-mesenchymal transition in cancer metastasis through the lymphatic system, Mol. Oncol. 11 (2017) 781–791.
[8] E. Sanchez-Tillo, Y. Liu, O. de Barrios, L. Siles, L. Fanlo, M. Cuatrecasas, D. S. Darling, D.C. Dean, A. Castells, A. Postigo, EMT-activating transcription factors in cancer: beyond EMT and tumor invasiveness, Cell. Mol. Life Sci. 69 (2012) 3429–3456.
[9] C.J. David, Y.H. Huang, M. Chen, J. Su, Y. Zou, N. Bardeesy, C.A. Iacobuzio-Donahue, J. Massague, TGF-beta tumor suppression through a lethal EMT, Cell 164 (2016) 1015–1103.
[10] W. Xue, L. Yang, C. Chen, M. Ashrafizadeh, Y. Tian, R. Sun, Wnt/β-catenin-driven EMT regulation in human cancers, Cell. Mol. Life Sci. 81 (2024) 79.
[11] E.M. De Francesco, M. Maggiolini, A.M. Musti, Crosstalk between notch, HIF-1α and GPER in breast cancer EMT, Int. J. Mol. Sci. 19 (2018) 2011.
[12] L. Peng, L. Wen, Q.-F. Shi, F. Gao, B. Huang, J. Meng, C.-P. Hu, C.-M. Wang, Scutellarin ameliorates pulmonary fibrosis through inhibiting NF-κB/NLRP3-mediated epithelial–mesenchymal transition and inflammation, Cell Death Dis. 11 (2020) 978.
[13] M. Li, X. Xu, J. Zhang, M. Liu, W. Wang, Y. Gao, Q. Sun, J. Zhang, Y. Lu, F. Wang, W. Liu, T. Zhou, Y. Yang, NudC-like protein 2 restrains centriole amplification by stabilizing HERC2, Cell Death Dis. 10 (2019) 628.
[14] Y. Yang, W. Wang, M. Li, Y. Gao, W. Zhang, Y. Huang, W. Zhuo, X. Yan, W. Liu, F. Wang, D. Chen, T. Zhou, NudCL2 is an Hsp90 cochaperone to regulate sister chromatid cohesion by stabilizing cohesin subunits, Cell. Mol. Life Sci. 76 (2019) 381–395.
[15] X. Xu, Y. Huang, F. Yang, X. Sun, R. Lin, J. Feng, M. Yang, J. Shao, X. Liu, T. Zhou, S. Xie, Y. Yang, NudCL2 is required for cytokinesis by stabilizing RCC2 with Hsp90 at the midbody, Protein Cell 15 (2024) 766–782.
[16] W. Chen, W. Wang, X. Sun, S. Xie, X. Xu, M. Liu, C. Yang, M. Li, W. Zhang, W. Liu, L. Wang, T. Zhou, Y. Yang, NudCL2 regulates cell migration by stabilizing both myosin-9 and LIS1 with Hsp90, Cell Death Dis. 11 (2020) 534.
[17] Y. Yang, X. Yan, Y. Cai, Y. Lu, J. Si, T. Zhou, NudC-like protein 2 regulates the LIS1/dynein pathway by stabilizing LIS1 with Hsp90, Proc. Natl. Acad. Sci. U. S. A. 107 (2010), 3499-350.
[18] M. Liu, W. Zhang, M. Li, J. Feng, W. Kuang, X. Chen, F. Yang, Q. Sun, Z. Xu, J. Hua, C. Yang, W. Liu, Q. Shu, Y. Yang, T. Zhou, S. Xie, NudCL2 is an autophagy receptor that mediates selective autophagic degradation of CP110 at mother centrioles to promote ciliogenesis, Cell Res. 31 (2021) 1199–1211.
[19] E. Lara-Pezzi, P.L. Majano, M. YaÂnÄez-MoÂ, M. GoÂmez-Gonzalo, M. Carretero, R. Moreno-Otero, F. SaÂnchez-Madrid, M. LoÂpez-Cabrera, Effect of the hepatitis B virus HBx protein on integrin-mediated adhesion to and migration on extracellular matrix, J. Hepatol. 34 (2001) 409–415.
[20] E.K. Paluch, I.M. Aspalter, M. Sixt, Focal adhesion-independent cell migration, Annu. Rev. Cell Dev. Biol. 32 (2016) 469–490.
[21] A. Malki, R.A. ElRuz, I. Gupta, A. Allouch, S. Vranic, A.E. Al Moustafa, Molecular mechanisms of colon cancer progression and metastasis: recent insights and advancements, Int. J. Mol. Sci. 22 (2020) 130.
[22] S. Haider, G. Meinhardt, P. Velicky, G.R. Otti, G. Whitley, C. Fiala, J. Pollheimer, M. Knofler, Notch signaling plays a critical role in motility and differentiation of human first-trimester cytotrophoblasts, Endocrinology 155 (2014) 263–274.
[23] S. Jiang, Y. Wang, Y. Wang, X. Yang, J. Yan, P. He, Q. L, X. Cao, Y. Huo, D. Liu, Z. Zhang, Y. Sun, Overexpressed EDIL3 predicts poor prognosis and promotes anchorage-independent tumor growth in human pancreatic cancer, Oncotarget 7 (2015) 4226–4240.
[24] S. Mukhopadhyay, A.C. Kimmelman, Autophagy is critical for cysteine metabolism in pancreatic cancer through regulation of SLC7A11, Autophagy 17 (2021) 1561–1562.
[25] W. Wang, Y. Zhang, X. Li, Q. E, Z. Jiang, Q. Shi, Y. Huang, J. Wang, Y. Huang, KCNA1 promotes the growth and invasion of glioblastoma cells through ferroptosis inhibition via upregulating SLC7A11, Cancer Cell Int. 24 (2024) 7.
[26] D. Li, M. Wan, X. Liu, S.C. Ojha, Y. Sheng, Y. Li, C. Sun, C. Deng, PART1 facilitates tumorigenesis and inhibits ferroptosis by regulating the miR-490-3p/SLC7A11 axis in hepatocellular carcinoma, Aging 16 (2024) 1339–11358.
[27] J. Chen, Z. Liu, Z. Wu, W. Li, X. Tan, Identification of a chemoresistance-related prognostic gene signature by comprehensive analysis and experimental validation in pancreatic cancer, Front. Oncol. 13 (2023) 113242.
[28] L. Sun, H. Dong, W. Zhang, N. Wang, N. Ni, X. Bai, N. Liu, Lipid Peroxidation, GSH depletion, and SLC7A11 inhibition are common causes of emt and ferroptosis in a549 cells, but different in specific mechanisms, DNA Cell Biol. 40 (2021) 172–183.
[29] S. Gui, W. Yu, J. Xie, L. Peng, Y. Xiong, Z. Song, H. Luo, J. Xiao, S. Yuan, Z. Cheng, SLC7A11 promotes EMT and metastasis in invasive pituitary neuroendocrine tumors by activating the PI3K/AKT signaling pathway, Endocr Connect 13 (2024) e240097.
[30] A. Nurmagambetova, V. Mustyatsa, A. Saidova, I. Vorobjev, Morphological and cytoskeleton changes in cells after EMT, Sci. Rep. 13 (2023) 22164.
[31] M. Li, X. Rao, Y. Cui, L. Zhang, X. Li, B. Wang, Y. Zheng, L. Teng, T. Zhou, W. Zhuo, The keratin 17/YAP/IL6 axis contributes to E-cadherin loss and aggressiveness of diffuse gastric cancer, Oncogene 41 (2022) 770–781.
[32] P. Koppula, L. Zhuang, B. Gan, Cystine transporter SLC7A11/xCT in cancer: ferroptosis, nutrient dependency, and cancer therapy, Protein Cell 12 (2021) 599–620.
[33] J. Deng, J. Zhang, Y. Ye, K. Liu, L. Zeng, J. Huang, L. Pan, M. Li, R. Bai, L. Zhuang, X. Huang, G. Wu, L. Wei, Y. Zheng, J. Su, S. Zhang, R. Chen, D. Lin, J. Zheng, N(6) -methyladenosine-mediated upregulation of wtapp1 promotes wtap translation and wnt signaling to facilitate pancreatic cancer progression, Cancer Res. 81 (2021) 5268–5528.
[34] N. Ferrand, E. Stragier, G. Redeuilh, M. Sabbah, Glucocorticoids induce CCN5/WISP-2 expression and attenuate invasion in oestrogen receptor-negative human breast cancer cells, Biochem. J. 447 (2012) 71–79.
[35] L. Mainsiouw, M.E. Ryan, S. Hafizi, J.C. Fleming, The molecular and clinical role of Tensin 1/2/3 in cancer, J. Cell Mol. Med. 27 (2023) 1763–1774.
[36] H. Chen, G. Xie, W. Wang, X. Yuan, W. Xing, J. Chen, M. Dou, L. Shen, Epigenetically downregulated semaphorin 3E contributes to gastric cancer, Oncotarget 6 (2015) 20449–20465.
[37] W. Wang, Y. Lin, G. Zhang, G. Shi, Y. Jiang, W. Hu, W. Zuo, circ_0002346 suppresses non-small-cell lung cancer progression depending on the regulation of the miR-582-3p/STXBP6 axis, Int J Genomics 2021 (2021) 1565660.
[38] C. Zheng, X. Yu, T. Xu, Z. Liu, Z. Jiang, J. Xu, J. Yang, G. Zhang, Y. He, H. Yang, X. Shi, Z. Li, J. Liu, W. Xu, KCTD4 interacts with CLIC1 to disrupt calcium homeostasis and promote metastasis in esophageal cancer, Acta Pharm. Sin. B 13 (2023) 4217–4233.
[39] T. Su, L. Huang, N. Zhang, S. Peng, X. Li, G. Wei, E. Zhai, Z. Zeng, L. Xu, FGF14 functions as a tumor suppressor through inhibiting pi3k/akt/mtor pathway in colorectal cancer, J. Cancer 11 (2020) 819–825.
[40] A. Kollara, P. Shathasivam, S. Park, M.J. Ringuette, T.J. Brown, Increased androgen receptor levels and signaling in ovarian cancer cells by VEPH1 associated with suppression of SMAD3 and AKT activation, J. Steroid Biochem. Mol. Biol. 196 (2020) 105498.
[41] A. Ota, A. Shiozaki, H. Shimizu, T. Kosuga, M. Kudou, K. Nishibeppu, T. Ohashi, T. Arita, H. Konishi, S. Komatsu, T. Kubota, H. Fujiwara, Y. Morinaga, E. Konishi, E. Otsuji, Functions and clinical significance of KCNB1 in esophageal squamous cell carcinoma, J. Gastroenterol. 60 (2025) 683–695.
[42] Z. Wang, Y. Ying, M. Wang, Q. Chen, Y. Wang, X. Yu, W. He, J. Li, S. Zeng, C. Xu, Comprehensive identification of onco-exaptation events in bladder cancer cell lines revealed L1PA2-SYT1 as a prognosis-relevant event, iScience 26 (2023) 108482.
[43] B. Schnabl, D. Valletta, G. Kirovski, C. Hellerbrand, Zinc finger protein 267 is up-regulated in hepatocellular carcinoma and promotes tumor cell proliferation and migration, Exp. Mol. Pathol. 91 (2011) 695–701.
[44] Z. Xiong, L. Yang, C. Zhang, W. Huang, W. Zhong, J. Yi, J. Feng, X. Zouxu, L. Song, X. Wang, MANF facilitates breast cancer cell survival under glucose-starvation conditions via PRKN-mediated mitophagy regulation, Autophagy 21 (2025) 80–101.
[45] X. Kaixuan, Z. Xiaobin, T. Jiaxuan, L. Shihui, W. Xinxin, H. Shuwei, D. Penggao, L. Xiang, Functional study of SAMD9L in familial gastric cancer, Turk. J. Gastroenterol. 34 (2023) 472–482.
[46] J. Ou, Q. Liao, Y. Du, W. Xi, Q. Meng, K. Li, Q. Cai, C.L.K. Pang, SERPINE1 and SERPINB7 as potential biomarkers for intravenous vitamin C treatment in non-small-cell lung cancer, Free Radic. Biol. Med. 209 (2023) 96–107.
[47] Z. Wang, Z. Wang, X. Niu, J. Liu, Z. Wang, L. Chen, B. Qin, Identification of seven-gene signature for prediction of lung squamous cell carcinom, OncoTargets Ther. 12 (2019) 5979–5988.